

## Supporting Information

### **Electrospun zirconia nanofibers for enhancing electrochemical synthesis of ammonia by artificial nitrogen fixation**

Jiaojiao Xia,<sup>a</sup> Haoran Guo,<sup>b</sup> Maozeng Cheng,<sup>a</sup> Chuyan Chen,<sup>a</sup> Minkang Wang,<sup>a</sup> Yong Xiang,<sup>a</sup> Tingshuai Li<sup>a\*</sup> and Enrico Traversa<sup>a\*</sup>

<sup>a</sup> School of Materials and Energy, University of Electronic Science and Technology of China, Chengdu 611731, Sichuan, China. E-mail: litingshuai@uestc.edu.cn; enrico.traversa@uestc.edu.cn

<sup>b</sup> School of Chemical Sciences, University of Chinese Academy of Sciences, 19 Yuquan Road, Shijingshan District, Beijing, 100049, China

**Table of Contents:**

**I. Computational Details .....S3**

**II. Experimental Section .....S4-S7**

**III. Supplementary Figures .....S8-S24**

**IV. Supplementary Table .....S25-S26**

**V. References.....S27-S28**

## I. Computational Details

Spin-polarized DFT calculations were performed by using the plane wave-based Vienna ab initio simulation package. The generalized gradient approximation method with Perdew–Burke–Ernzerhof functional <sup>[1]</sup> was used to describe the exchange–correlation interaction among electrons. The van der Waals correction with the Grimme approach (DFT-D3) <sup>[2]</sup> was included in the interaction between single molecule/atoms and substrates. The energy cutoff for the plane wave–basis expansion was set to 450 eV and the atomic relaxation was continued until the forces acting on atoms were smaller than 0.02 eV Å<sup>-1</sup>. The Brillouin zone was sampled with 2 × 2 × 1 Gamma-center *k*-point mesh, and the electronic states were smeared using the Fermi scheme with a broadening width of 0.1 eV. The free energies of the reaction intermediates were obtained by  $\Delta G = \Delta E_{\text{ads}} + \Delta \text{ZPE} - T\Delta S$ , where  $\Delta E_{\text{ads}}$  is the adsorption energy, ZPE is the zero-point energy, and *S* is the entropy at 298 K. In this study, the entropies of molecules in the gas phase were obtained from the literature. <sup>[3]</sup>

## II. Experimental Section

### Material characterizations:

X-ray diffraction (XRD) analysis was performed by a Bruker D8 Advance diffractometer at 40 kV, and the radiation was Cu K $\alpha$  ( $\lambda = 1.5418$  Å). The microstructure images were from FEI SCIOS Dual Beam scanning electron microscope operated at 20 kV. The transmission electron microscopy (TEM) and high-resolution TEM (HRTEM) images of sintered fibers were obtained from FEI F30 equipment with the accelerating voltage of 300 kV and the elemental analysis was measured by ICP-OES (Agilent ICPOES730). X-ray photoelectron spectroscopy (XPS) measurements were conducted by a Escalab 250Xi (Thermo Fisher) X-ray photoelectron spectrometer using Al as the exciting source. BET surface area was tested by ASAP 2460. Nuclear magnetic resonance (NMR) was tested on a Bruker 400 MHz instrument.

### Working electrode preparation:

5 mg ZrO<sub>2</sub> nanofiber grinded into powder and 20  $\mu$ L of 5 wt% Nafion solution were added into a mixed solution containing 325  $\mu$ L deionized water and 655  $\mu$ L ethanol, followed by 30 min ultrasonic dispersion to form a homogeneous suspension. Then, 20  $\mu$ L of such suspension was dropped on a 1\*1 cm<sup>2</sup> carbon paper and dried in ambient temperature. The loading mass of catalyst on such resulting electrode is 0.1 mg and all

electrochemical measurements were performed under identical conditions with the same catalyst mass loading.

#### **Process of the Nafion membrane:**

Step 1: Boiling it in a 3 wt% H<sub>2</sub>O<sub>2</sub> solution at 80 °C for 1 h. Step 2: Washing it in deionized water several times. Step 3: Boiling it for 1 h in 80 °C sulfuric acid. Step 4: Soaking it for 30 min and repeating several times in deionized water.

#### **Determination of ammonia (NH<sub>3</sub>):**

Typically, the indophenol blue method<sup>[4]</sup> was adopted to quantify the NH<sub>3</sub> in 0.1 M electrolyte. In 0.1M HCl and 0.1 M KOH, firstly, 2 mL of the electrolyte taken from cathode was mixed with 2 mL 1 M NaOH solution containing 5% trisodium citrate and 5% salicylic acid. Then, 1 mL 0.05 M NaClO solution was added into such mixed solution. Finally, 0.2 mL 1% C<sub>5</sub>FeN<sub>6</sub>Na<sub>2</sub>O was added. After standing for 2h without exposure, such solution was identified via UV-Vis spectroscopy at the wavelength of 655 nm. The NH<sub>3</sub> yields were quantified by the standard curves ( $Y_{HCl} = 0.39297X_{HCl} + 0.04349$ ,  $Y_{KOH} = 0.42286X_{KOH} + 0.03943$ ). When tested in 0.1 M Na<sub>2</sub>SO<sub>4</sub>, 4 mL the electrolyte was taken from the cathode chamber and was mixed with 50 μL oxidizing solution prepared by NaClO (ρCl = 4–4.9) and 0.75 M NaOH, 500 μL coloring solution (0.4 M C<sub>7</sub>H<sub>5</sub>O<sub>3</sub>Na and 0.32 M NaOH), and 50 μL catalyst solution (1 wt% Na<sub>2</sub>[Fe(CN)<sub>5</sub>NO]<sub>2</sub>H<sub>2</sub>O). After standing in a lightless environment

at ambient temperatures for 1 h, such solution was analyzed via the UV-Vis spectroscopy at the wavelength of 655 nm. The standard curve is  $Y = 0.55500X + 0.01546$  ( $R^2=0.999$ ), which was calibrated using a standardized  $\text{NH}_4\text{Cl}$  solution with five progressive concentrations.

#### **Determination of hydrazine ( $\text{N}_2\text{H}_4$ ):**

The hydrazine was identified using the Watt and Chrisp method. [5] Typically, 5 mL electrolyte solution was added with 5 mL hydrazine chromogenic agent prepared by 5.99 g  $\text{C}_9\text{H}_{11}\text{NO}$ , 30 mL  $\text{HCl}$  and 300 mL ethanol. Followed by 20 min complete stir, the absorbance of such solution at the wavelength of 455 nm was measured to quantify the hydrazine yields with a standard curve of hydrazine ( $y = 2.49635x + 0.16741$ ,  $R^2 = 0.9994$ ).

#### **Calculations of $\text{NH}_3$ faradaic efficiency (FE) and $\text{NH}_3$ yield rate:**

The FE was calculated by equation (1):

$$FE = \frac{3 \times F \times [\text{NH}_3] \times V}{17 \times Q} \quad (1)$$

The yield of  $\text{NH}_3$  was calculated by equation (2):

$$\text{NH}_3 \text{ yield} = \frac{[\text{NH}_3] \times V}{t \times m_{\text{cat.}}} \quad (2)$$

where 3 is the number of the electrons transferred for one  $\text{NH}_3$  molecule production,  $F$  is the Faraday constant,  $[\text{NH}_3]$  is the measured  $\text{NH}_3$  concentration,  $V$  is the volume of electrolyte in the cathode chamber, 17 is the molar mass of  $\text{NH}_3$ ,  $Q$  is the quantity of applied charge/electricity,  $t$  is the testing time, and  $m_{\text{cat.}}$  is the loading mass of catalyst.

### **$^{15}\text{N}_2$ isotope labeling experiments:**

An isotopic labeling experiment using  $^{15}\text{N}_2$  (purchased from Sigma-Aldrich Chemical Reagent Co., 98 atom %  $^{15}\text{N}$ ) as the feed gas was conducted to elucidate the activity origin of  $\text{ZrO}_2(\text{V}_\text{O})\text{NF}$ . The  $^{15}\text{N}_2$  gas was purified by passing through an acid trap (0.1 M HCl) before entering the reaction chamber with 10 mL of electrolyte. After  $^{15}\text{NRR}$  for 2 h at  $-0.7$  V vs. RHE in 0.1 M  $\text{Na}_2\text{SO}_4$  solution, the obtained  $^{15}\text{NH}_4^+$  electrolyte was analyzed using  $^1\text{H}$  nuclear magnetic resonance (NMR, 400 MHz). To prepare the NMR sample, 600  $\mu\text{L}$  solution concentrating from 1.8 mL of electrolyte after  $^{15}\text{NRR}$  was firstly acidified with 3 M HCl to achieve pH  $\sim 1-2$ , then 400  $\mu\text{L}$  of 100 ppm dimethyl sulfoxide (DMSO) were added. Similarly, the amount of  $^{14}\text{NH}_4^+$  was determined by this method when  $^{14}\text{N}_2$  (99.999%) was used as the feed gas. All NMR measurements were carried out with water suppression and 5000 scans.

### III. Supplementary Figures

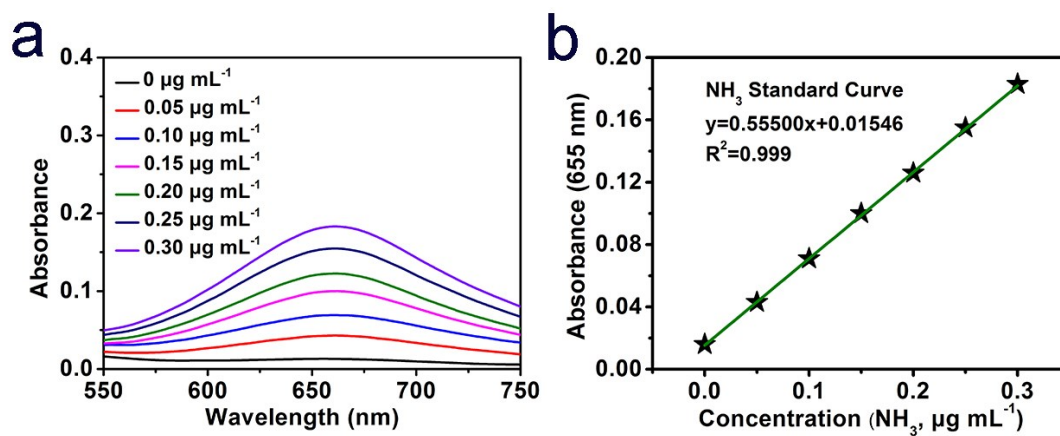


Fig. S1. (a) UV-Vis absorption spectra of indophenol assays performed with different concentrations of  $\text{NH}_3$  in  $0.1 \text{ M Na}_2\text{SO}_4$ . (b) A calibration curve used for estimating the  $\text{NH}_3$  concentration.

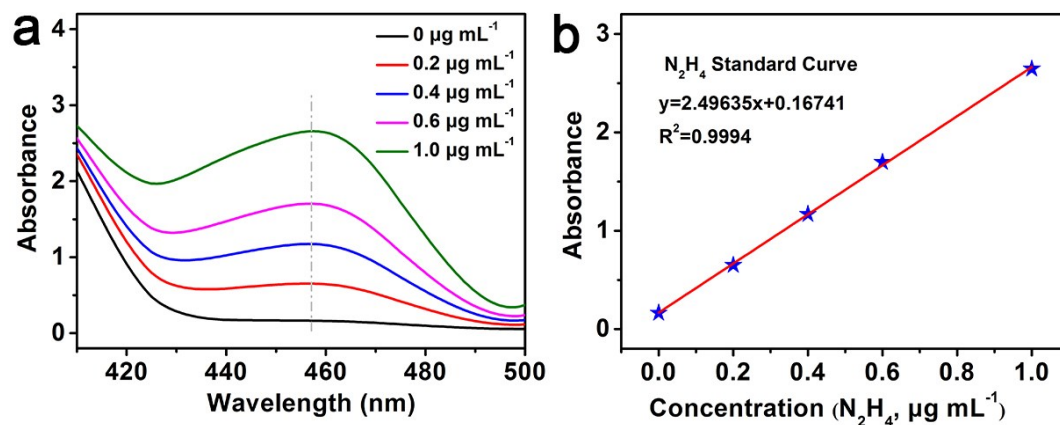


Fig. S2. (a) UV-Vis spectra of various  $\text{N}_2\text{H}_4$  concentrations after adding into chemical indicator by the Watt and Chrisp method. (b) A calibration curve used for the calculation of  $\text{N}_2\text{H}_4$  concentrations.

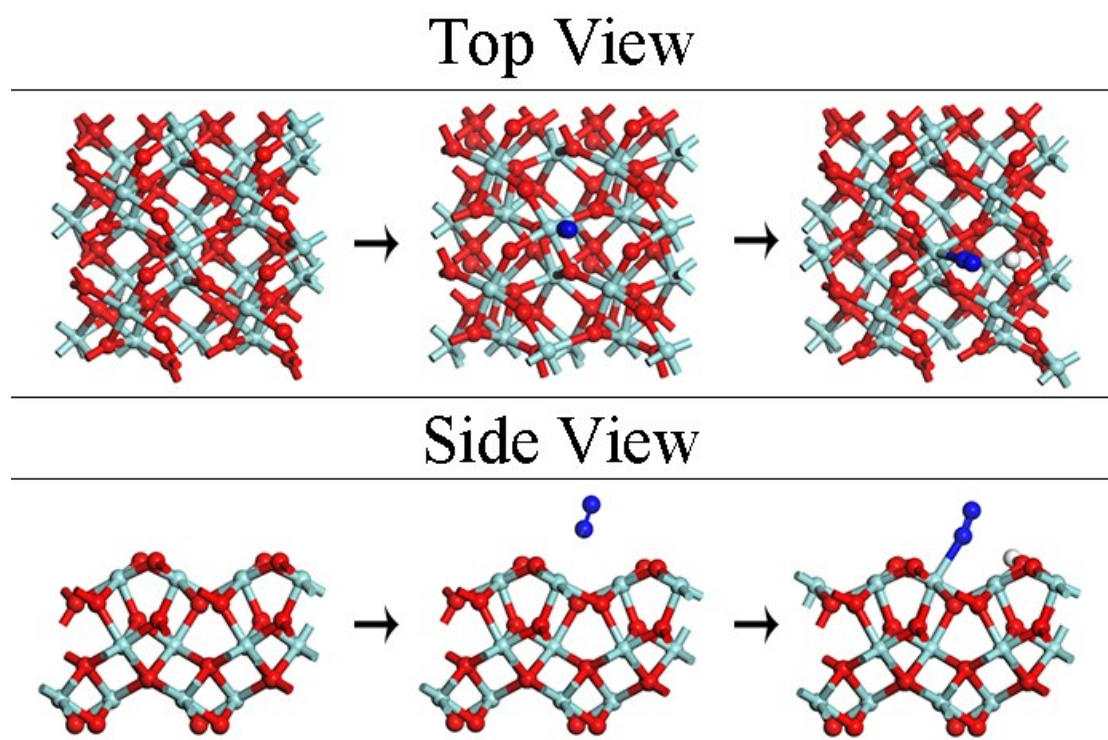


Fig. S3. The N<sub>2</sub> adsorption processes in top and side views of the pristine ZrO<sub>2</sub> (100) surfaces.

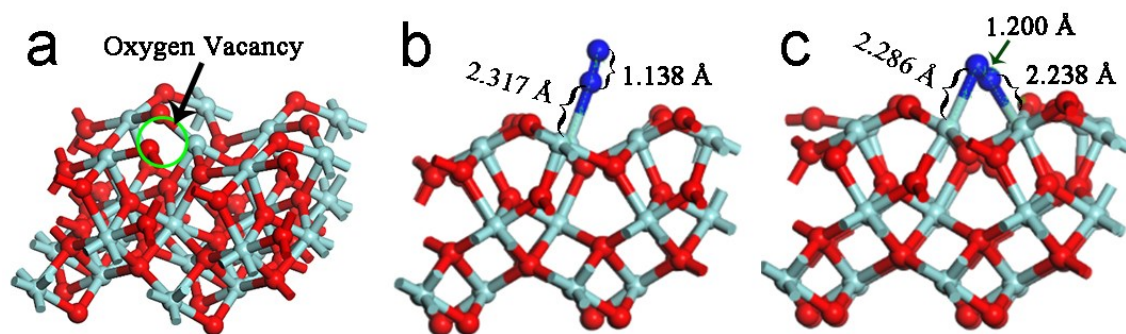


Fig. S4. (a)  $\text{ZrO}_2$  with oxygen vacancies (100) surface.  $\text{N}_2$  molecules are attached to Zr atoms with oxygen vacancies on the (100) surfaces by end contact (b) and side contact (c). The N-N and N-Zr bond length are showed.

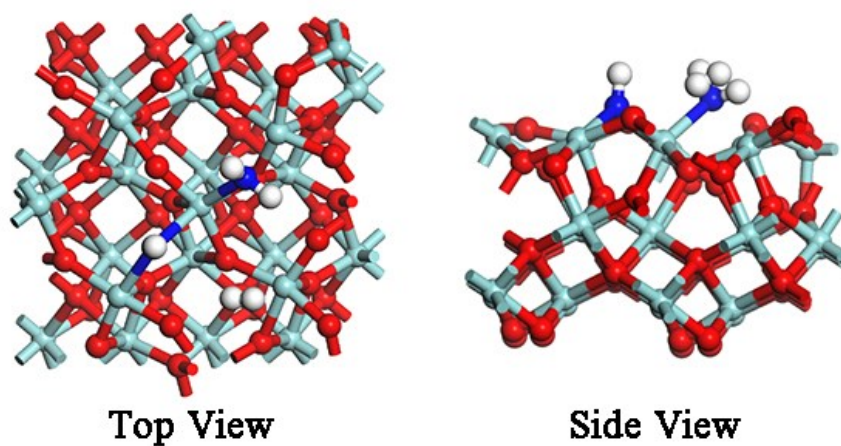


Fig. S5. N<sub>2</sub> molecules are adsorbed at the active site by side contact of an alternate pathway from the top and side views of ZrO<sub>2</sub> with oxygen vacancies (100) surfaces.

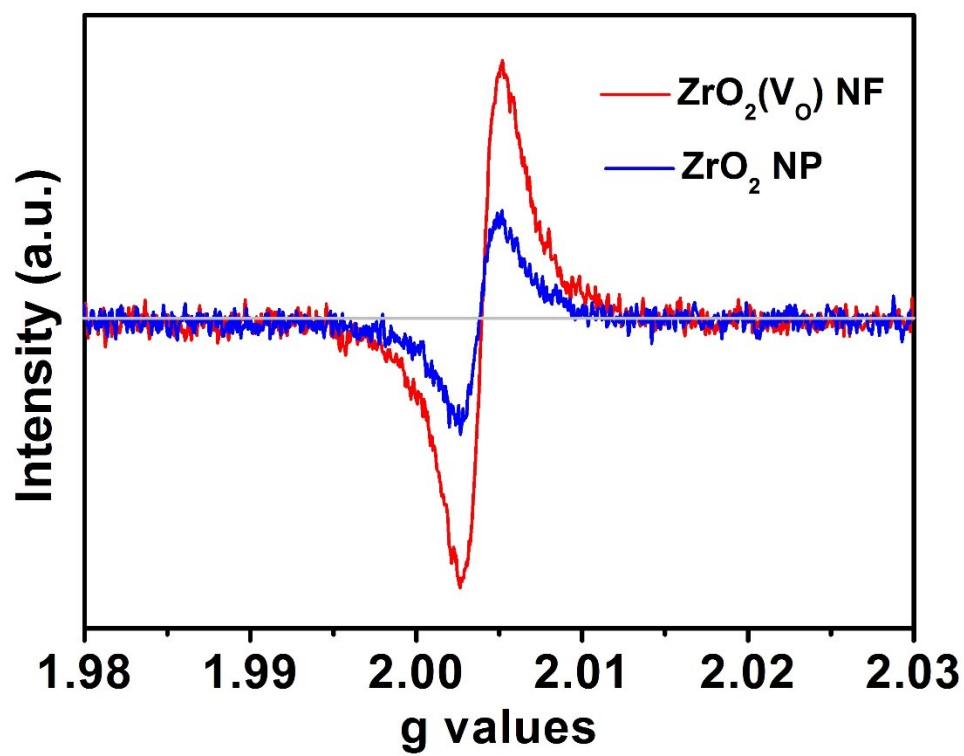


Fig. S6. ESR spectra of ZrO<sub>2</sub>(V<sub>O</sub>) NFs and ZrO<sub>2</sub> NPs.

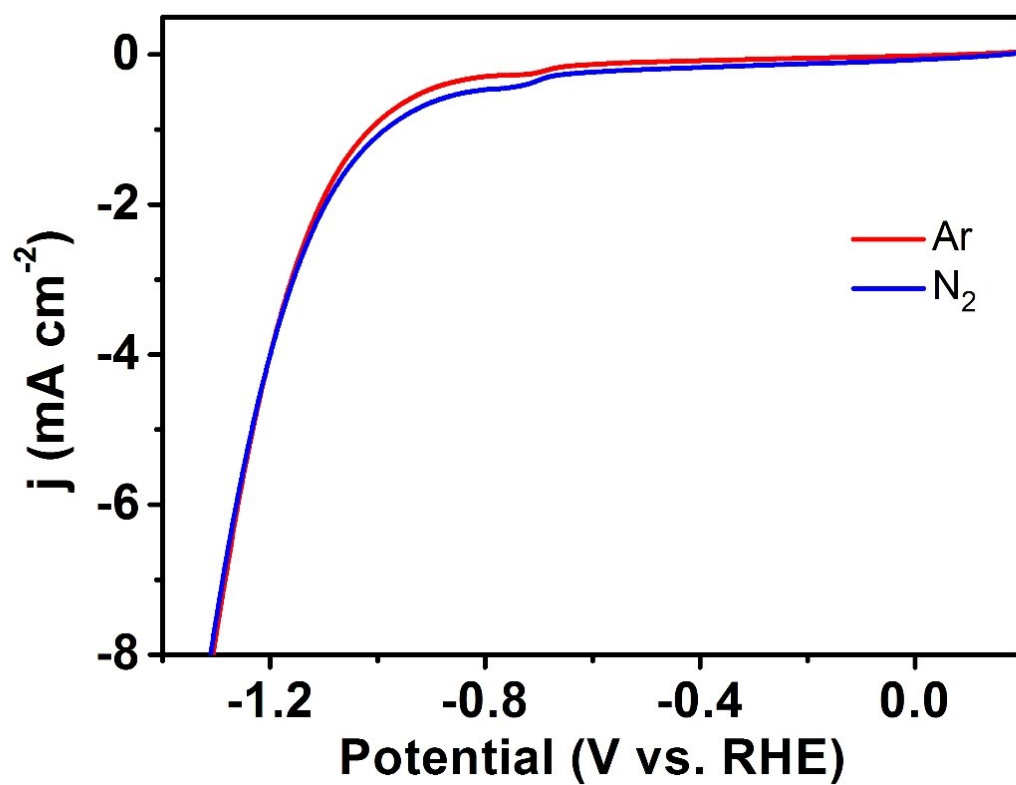


Fig. S7. LSV curves of  $\text{ZrO}_2(\text{V}_\text{O})\text{NF}$  in Ar- and  $\text{N}_2$ -saturated 0.1 M  $\text{Na}_2\text{SO}_4$  at the scan rate of 5 mV/s.

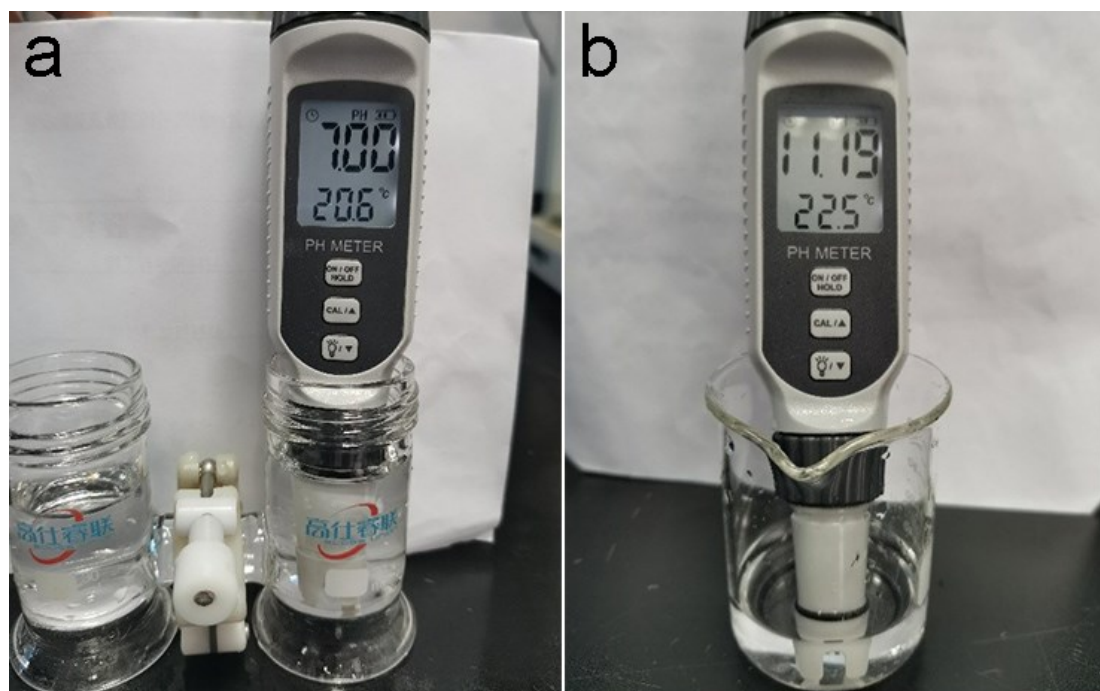


Fig. S8. The pH value of the electrolyte (a) before and (b) after NRR electrolytic process.

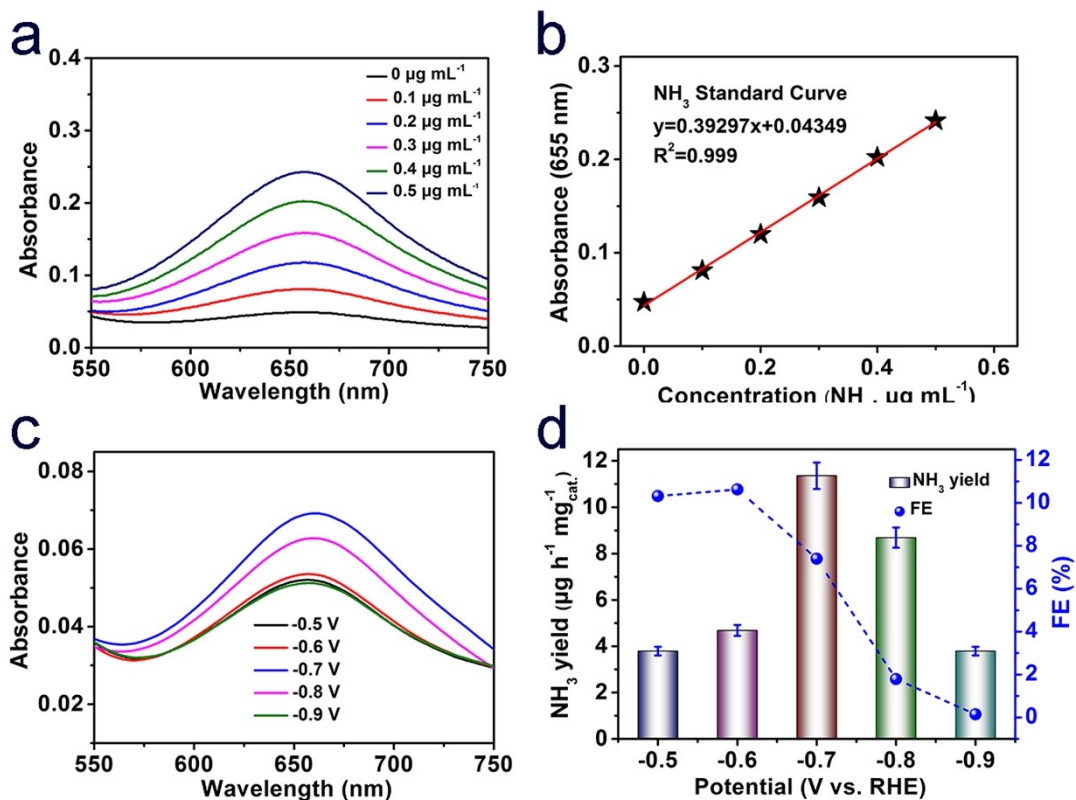


Fig. S9. (a) UV-Vis absorption spectra of indophenol assays with  $\text{NH}_4\text{Cl}$  after incubation for 2 h at room temperature in 0.1 M HCl. (b) Calibration curve used for estimation of  $\text{NH}_3$  by  $\text{NH}_4\text{Cl}$  concentration in 0.1 M HCl. (c) UV-vis absorption spectra of the electrolytes stained with indophenol indicator and (d)  $\text{NH}_3$  production rates with FEs for  $\text{ZrO}_2(\text{V}_\text{O})$  NFs at five different potentials for 2 h in 0.1 M HCl.

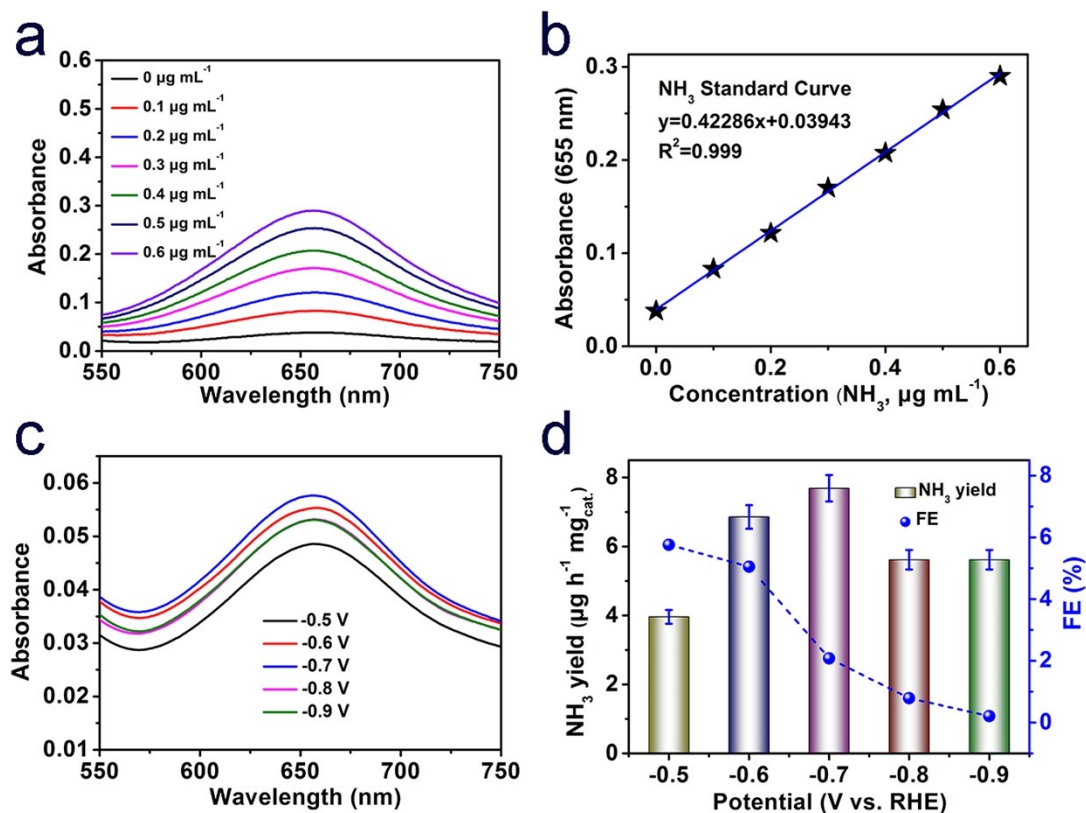


Fig. S10. (a) UV-Vis absorption spectra of indophenol assays with  $\text{NH}_4\text{Cl}$  after incubation for 2 h at room temperature in 0.1 M KOH. (b) Calibration curve used for estimation of  $\text{NH}_3$  by  $\text{NH}_4\text{Cl}$  concentration in 0.1 M KOH. (c) UV-vis absorption spectra of the electrolytes stained with indophenol indicator and (d)  $\text{NH}_3$  production rates with FEs for  $\text{ZrO}_2(\text{V}_0)$  NFs at five different potentials for 2 h in 0.1 M KOH.

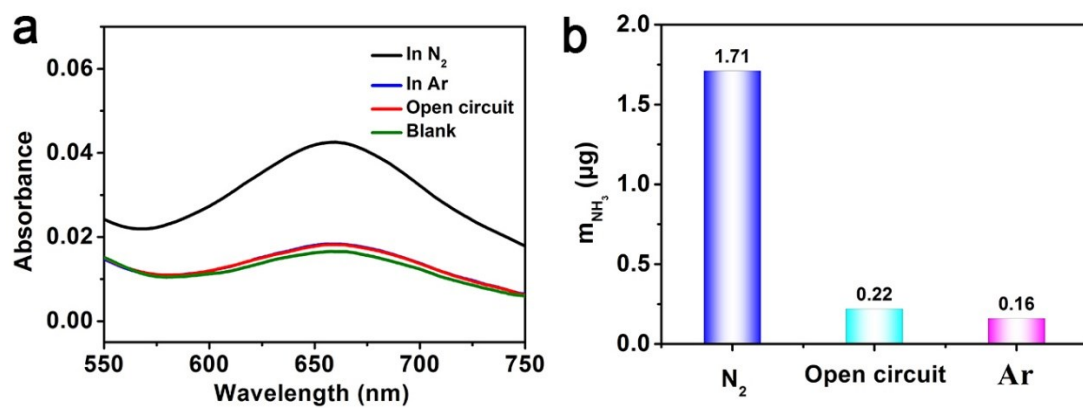


Fig. S11. (a) UV-Vis absorption spectra of indophenol assays and (b) corresponding ammonia yield after 2-h electrolysis in 0.1 M Na<sub>2</sub>SO<sub>4</sub> under different condition for ZrO<sub>2</sub>(V<sub>O</sub>) NFs.

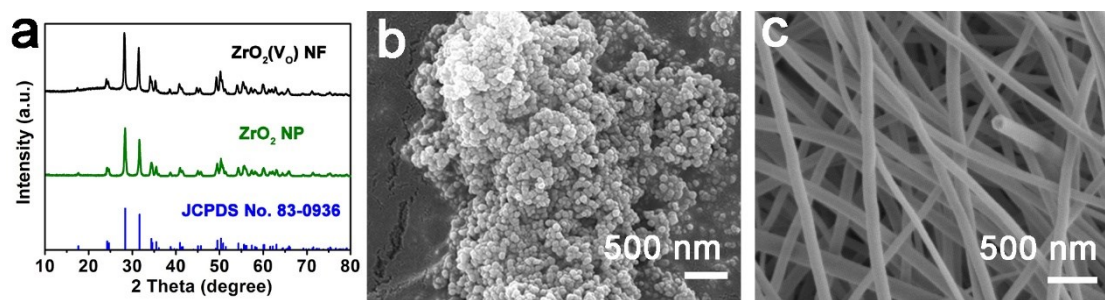


Fig. S12. (a) XRD patterns of  $\text{ZrO}_2(\text{V}_\text{O})$  NFs and  $\text{ZrO}_2$  NPs. (b) SEM micrograph of  $\text{ZrO}_2$  NPs. (c) SEM micrograph of  $\text{ZrO}_2$  NFs.

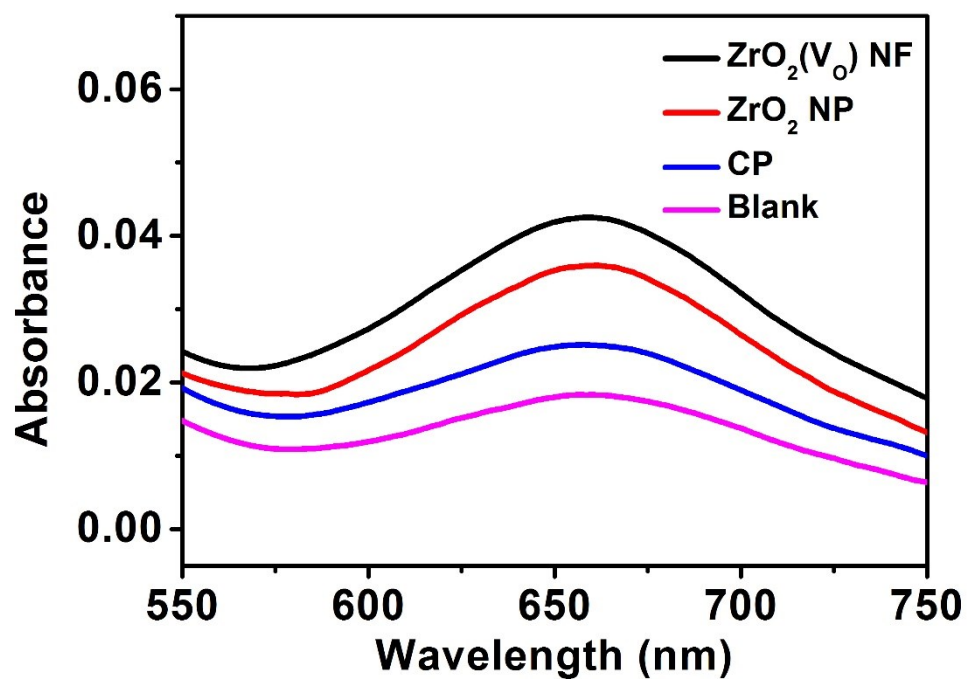


Fig. S13. The UV-Vis absorption spectra of indophenol assays with electrolyte of ZrO<sub>2</sub>(V<sub>0</sub>) NFs, ZrO<sub>2</sub> NPs and CPs after 2-h electrolysis.

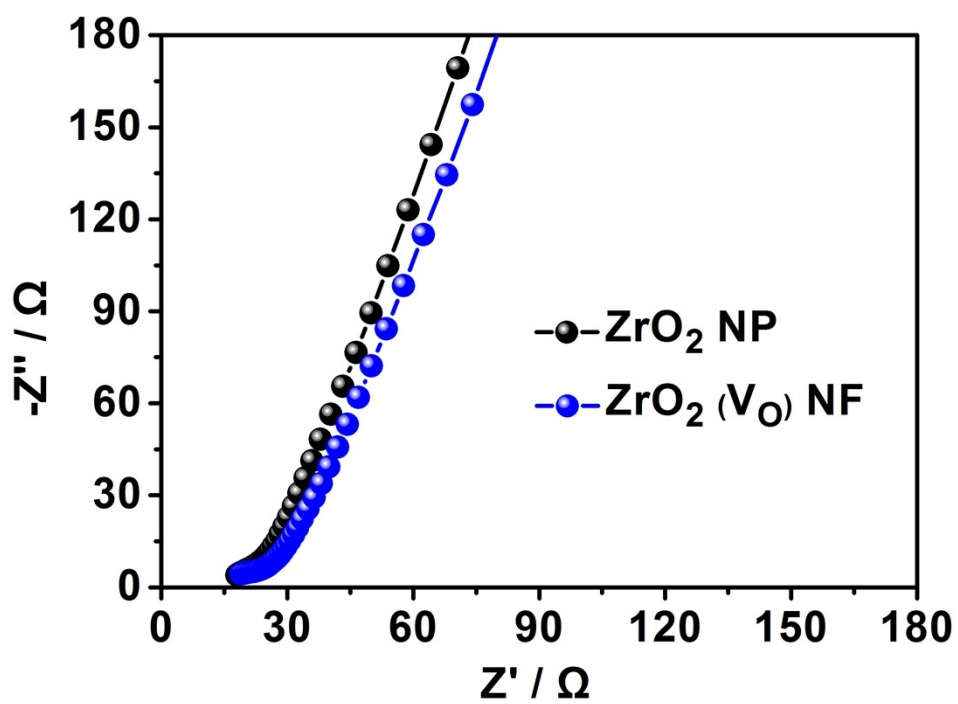


Fig. S14. EIS of the  $\text{ZrO}_2(\text{V}_\text{O})$  NFs and  $\text{ZrO}_2$  NPs in 0.1 M  $\text{N}_2$ -saturated  $\text{Na}_2\text{SO}_4$ . For comparison, the  $R_\Omega$  was omitted in the Nyquist plots.

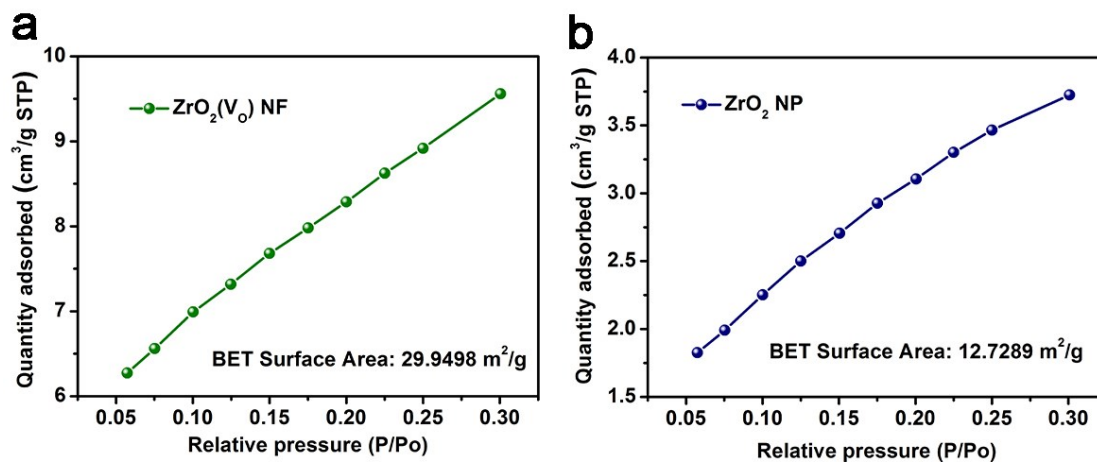


Fig. S15. N<sub>2</sub> adsorption isotherms of (a) ZrO<sub>2</sub>(V<sub>o</sub>) NFs and (b) ZrO<sub>2</sub> NPs.

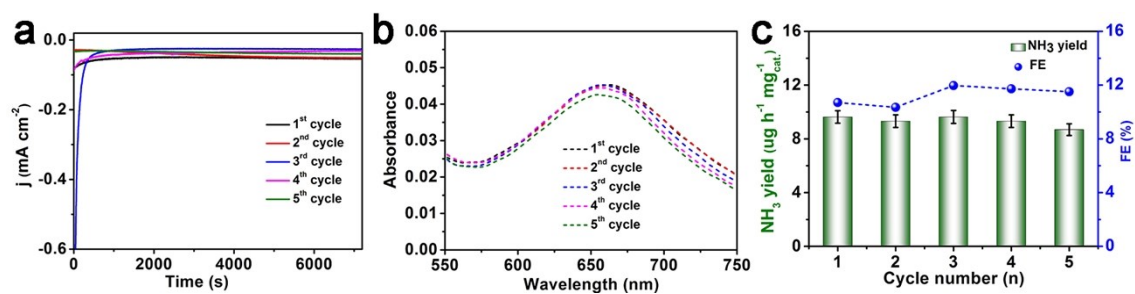


Fig. S16. (a) Time-dependent current density curves, (b) UV-Vis absorption spectra of the electrolytes stained with indophenol indicator after NRR electrolysis and (c) NH<sub>3</sub> rate with FEs for ZrO<sub>2</sub>(VO) NFs during five identical NRR tests at -0.7 V.

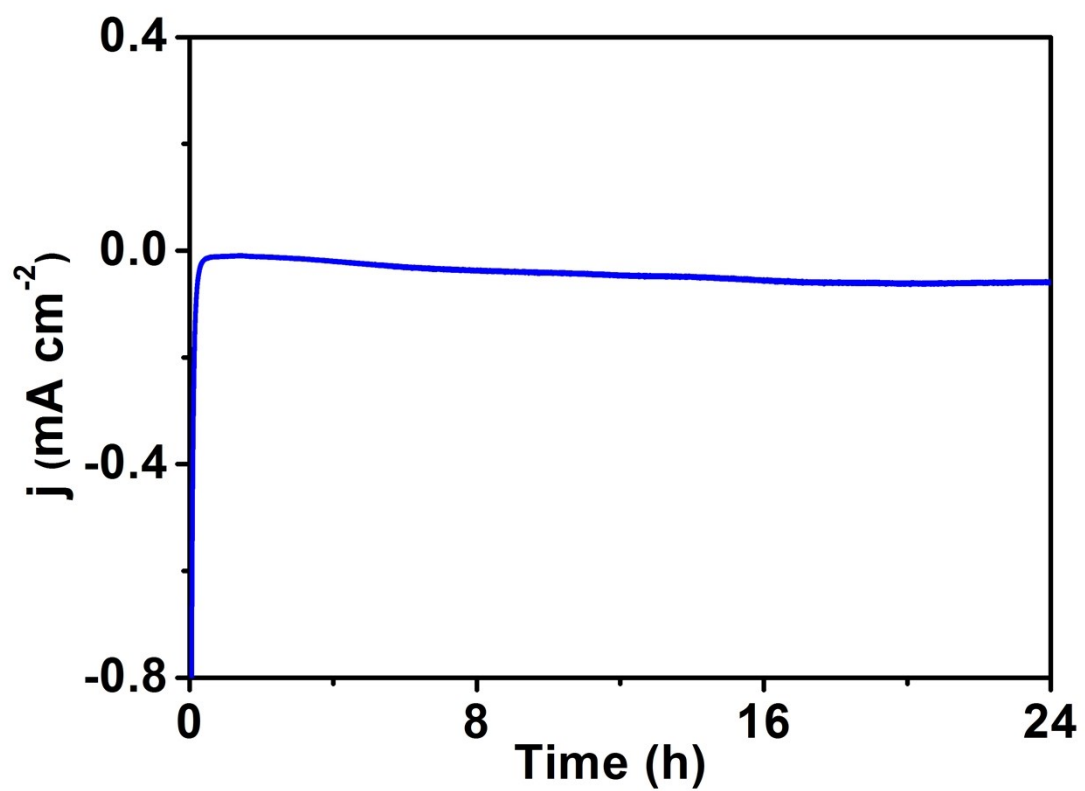


Fig. S17. Chronoamperometric test for  $\text{ZrO}_2(\text{V}_\text{O})$  NFs at  $-0.7$  V for 24 h.

#### IV. Supplementary Table

**Table S1** Comparison of electrocatalytic N<sub>2</sub> reduction performance for ZrO<sub>2</sub> NF with other electrocatalysts under ambient conditions.

Catalyst	Electrolyte	NH <sub>3</sub> yield	FE%	Ref.
ZrO <sub>2</sub> NF	0.1 M Na <sub>2</sub> SO <sub>4</sub>	9.62973 ± 0.48 μg h <sup>-1</sup> mg <sup>-1</sup> <sub>cat.</sub>	11.968 ±0.59	This work
TiO <sub>2</sub>	0.1M Na <sub>2</sub> SO <sub>4</sub>	9.16×10 <sup>-11</sup> mol s <sup>-1</sup> cm <sup>-2</sup>	2.5	[6]
d-TiO <sub>2</sub>	0.1M HCl	1.24×10 <sup>-10</sup> mol s <sup>-1</sup> cm <sup>-2</sup>	9.17	[7]
MoO <sub>3</sub>	0.1M HCl	4.80×10 <sup>-10</sup> mol s <sup>-1</sup> cm <sup>-2</sup>	1.9	[8]
γ-Fe <sub>2</sub> O <sub>3</sub>	0.1M KOH	12.5 nmol h <sup>-1</sup> mg <sup>-1</sup>	1.9	[9]
Fe <sub>3</sub> O <sub>4</sub> /Ti	0.1M Na <sub>2</sub> SO <sub>4</sub>	5.6 × 10 <sup>-11</sup> mol s <sup>-1</sup> cm <sup>-2</sup>	2.6	[10]
Fe <sub>2</sub> O <sub>3</sub> nanorods	0.1M Na <sub>2</sub> SO <sub>4</sub>	15.9 μg h <sup>-1</sup> mg <sup>-1</sup> <sub>cat.</sub>	0.94	[11]
CuO/rGO	0.1M Na <sub>2</sub> SO <sub>4</sub>	1.8 × 10 <sup>-10</sup> mol s <sup>-1</sup> cm <sup>-2</sup>	3.9	[12]
SnO <sub>2</sub>	0.1M Na <sub>2</sub> SO <sub>4</sub>	4.03 μg h <sup>-1</sup> mg <sup>-1</sup> <sub>cat.</sub>	2.17	[13]
MnO	0.1M Na <sub>2</sub> SO <sub>4</sub>	7.92 μg h <sup>-1</sup> mg <sup>-1</sup> <sub>cat.</sub>	8.02	[14]

$\alpha$ -Au/CeO <sub>x</sub> -RGO	0.1 M HCl	8.31 $\mu\text{g h}^{-1} \text{mg}^{-1}_{\text{cat}}$	10.1	[15]
V <sub>2</sub> O <sub>3</sub> /C	0.1M Na <sub>2</sub> SO <sub>4</sub>	12.3 $\mu\text{g h}^{-1} \text{mg}^{-1}_{\text{cat}}$	7.28	[16]
Ru/CeO <sub>2</sub> -V <sub>0</sub>	0.05 M H <sub>2</sub> SO <sub>4</sub>	$9.87 \times 10^{-8} \text{ mmol s}^{-1} \text{ cm}^{-2}$	11.7	[17]
C@YSZ	0.1M Na <sub>2</sub> SO <sub>4</sub>	24.6 $\mu\text{g h}^{-1} \text{mg}^{-1}_{\text{cat}}$	8.2	[18]
Mo-doped W <sub>18</sub> O <sub>49</sub>	0.1M Na <sub>2</sub> SO <sub>4</sub>	5.3 $\mu\text{g h}^{-1} \text{mg}^{-1}_{\text{cat}}$	12.1	[19]
P-NiO/CC	0.1 M Na <sub>2</sub> SO <sub>4</sub>	29.1 $\mu\text{g h}^{-1} \text{mg}^{-1}_{\text{cat}}$	10.8	[20]

## V. References

- [1] J. P. Perdew, K. Burke and M. Ernzerhof, *Phys. Rev. Lett.*, 1996, **77**, 3865–3868.
- [2] S. Grimme, J. Antony, S. Ehrlich and H. Krieg, *J. Chem. Phys.*, 2010, **132**, 154104.
- [3] <https://janaf.nist.gov/> (accessed: January 2019).
- [4] D. Zhu, L. Zhang, R. E. Ruther and R. J. Hamers, *Nat. Mater.*, 2013, **12**, 836–841.
- [5] G. W. Watt and J. D. Chrisp, *Anal. Chem.*, 1952, **24**, 2006–2008.
- [6] R. Zhang, X. Ren, X. Shi, Fe. Xie, B. Zheng, X. Guo and X. Sun, *ACS Appl. Mater. Interfaces*, 2018, **10**, 28251–28255.
- [7] L. Yang, T. Wu, R. Zhang, H. Zhou, L. Xia, X. Shi, H. Zheng, Y. Zhang and X. Sun, *Nanoscale*, 2019, **11**, 1555–1562.
- [8] J. Han, X. Ji, X. Ren, G. Cui, L. Li, F. Xie, H. Wang, B. Li and X. Sun, *J. Mater. Chem. A*, 2018, **6**, 12974–12977.
- [9] J. Kong, A. Lim, C. Yoon, J. H. Jang, H. C. Ham, J. Han, S. Nam, D. Kim, Y. E. Sung, J. Choi and H. S. Park, *ACS. Sustainable. Chem. Eng.*, 2017, **5**, 10986–10996.
- [10] Q. Liu, X. Zhang, B. Zhang, Y. Luo, G. Cui, F. Xie and X. Sun, *Nanoscale*, 2018, **10**, 14386–14389.
- [11] X. Xiang, Z. Wang, X. Shi, M. Fan and X. Sun, *Chem. Cat. Chem.*,

2018, **20**, 4530–4535.

[12] F. Wang, Y. Liu, H. Zhang, K. Chu, *Chem. Cat. Chem.*, 2019, **11**, 1441–1447.

[13] L. Zhang, X. Ren, Y. Luo, X. Shi, A. M. Asiri, T. Li, X. Sun, *Chem. Commun.*, 2018, **54**, 12966–12969.

[14] Z. Wang, F. Gong, L. Zhang, R. Wang, L. Ji, Q. Liu, Y. Luo, H. Guo, Y. Li, Peng Gao, X. Shi, B. Li, B. Tang, X. Sun, *Adv. Sci.*, 2019, **6**, 1801182.

[15] S. Li, D. Bao, M. Shi, B. Wulan, J. Yan and Q. Jiang, *Adv. Mater.*, 2017, **29**, 1700001.

[16] R. Zhang, J. Han, B. Zheng, X. Shi, A. M. Asiri, X. Sun, *Inorg. Chem. Front.*, 2019, **6**, 391–395.

[17] Y. Ding, L. Huang, J. Zhang, A. Guan, Q. Wang, L. Qian, L. Zhang and G. Zheng, *J. Mater. Chem. A*, 2020, **8**, 7229-7234.

[18] S. Luo, X. Li, M. Wang, X. Zhang, W. Gao, S. Su, G. Liu and M. Luo, *J. Mater. Chem. A*, 2020, **8**, 5647–5654.

[19] M. Yang, R. Huo, H. Shen, Q. Xia, J. Qiu, A. W. Robertson, X. Li and Z. Sun, *ACS Sustainable Chem. Eng.*, 2020, **8**, 2957–2963.

[20] Y. Li, Y. Liu, J. Wang, Y. Guo and K. Chu, *Inorg. Chem. Front.*, 2020, **7**, 455-463.